2008

Extraction of Impervious Surface Areas from High Spatial Resolution Imagery by Multiple Agent Segmentation and Classification

Yuyu Zhou

Yeqiao Wang
University of Rhode Island, yqwang@uri.edu

Citation/Publisher Attribution

Wang, Y. (2008). Extraction of Impervious Surface Areas from High Spatial Resolution Imagery by Multiple Agent Segmentation and Classification. *Photogrammetric Engineering & Remote Sensing*, *7*, 857-868.
https://doi.org/10.14358/PERS.74.7.857
Available at: https://doi.org/10.14358/PERS.74.7.857

Extraction of Impervious Surface Areas from High Spatial Resolution Imagery by Multiple Agent Segmentation and Classification

Creative Commons License

This work is licensed under a Creative Commons Attribution-Noncommercial-No Derivative Works 4.0 License.

Extraction of Impervious Surface Areas from High Spatial Resolution Imagery by Multiple Agent Segmentation and Classification

[This Paper was the Winner of the 2007 BAE Systems Award Given at the ASPRS 2007 Annual Conference]

Yuyu Zhou and Y.Q. Wang

Abstract

In recent years impervious surface areas (ISA) have emerged as a key paradigm to explain and predict ecosystem health in relationship to watershed development. The ISA data are essential for environmental monitoring and management in coastal State of Rhode Island. However, there is lack of information on high spatial resolution ISA. In this study, we developed an algorithm of multiple agent segmentation and classification (MASC) that includes submodels of segmentation, shadow-effect, MANOVA-based classification, and post-classification. The segmentation sub-model replaced the spectral difference with heterogeneity change for regions merging. Shape information was introduced to enhance the performance of ISA extraction. The shadow-effect sub-model used a split-and-merge process to separate shadows and the objects that cause the shadows. The MANOVA-based classification sub-model took into account the relationship between spectral bands and the variability in the training objects and the objects to be classified. Existing GIS data were used in the classification and post-classification process. The MASC successfully extracted ISA from high spatial resolution airborne true-color digital orthophoto and space-borne QuickBird-2 imagery in the testing areas, and then was extended for extraction of high spatial resolution ISA in the State of Rhode Island.

Introduction

Impervious surface areas (ISA) are defined as any impenetrable material that prevents infiltration of water into the soil. Urban pavements, such as rooftops, roads, sidewalks, parking lots, driveways, and other manmade concrete surfaces are among impervious surface types that featured the urban and suburban landscape. ISA have been considered as a key environmental indicator due to its impacts on water systems and its role in transportation and concentration of pollutants (Arnold and Gibbons, 1996). Urban runoff, mostly through impervious surface, is the leading source of pollution in the Nation's estuaries, lakes, and rivers (Arnold and Gibbons, 1996; Booth and Jackson, 1997). A recently published watershed-planning model predicts that most stream quality indicators decline when watershed ISA exceed 10 percent (Schueler, 2003). ISA have also been recognized as an indicator of intensity of urban environment. With advent of urban sprawl ISA have been identified as a key issue in habit health (Brabec *et al.*, 2002). Quantification of the percentage of impervious surface in landscape has become increasingly important with growing concern of its impact on the environment (Weng, 2001; Civco *et al.*, 2002; Dougherty *et al.*, 2004; Wang and Zhang, 2004).

As a result of urban land development, the coastal State of Rhode Island experiences problems caused by urban runoff. The most recent significant example occurred in the state was on 21 August 2003, over one million fish as well as other marine life in Greenwich Bay were killed due to the lack of oxygen in the water. The impervious surface is considered as one of the possible factors that triggered this incident. However, there is lack of information on high spatial resolution ISA in the state. A previous study using Landsat remote sensing data revealed the increasing urban land-use and land-cover (Novak and Wang, 2004) but was not able to obtain precise ISA coverage with 30-meter pixel size.

Conventionally, manual delineation through aerial photography has been used to extract ISA information (Draper and Rao, 1986). For example, currently available land-use and land-cover data for the state were developed based on manual interpretation of 1987 and 1995 aerial photography data, respectively. However, manual delineation is labor-intensive, prohibitively expensive for large area, and difficult to keep the interpretation results consistent. In addition, ISA are not a separate class in general purpose land-use and land-cover maps. ISA can be obtained from classification of remote sensing data. Due to limitations of spectral mixing and spatial resolutions, the accuracy of ISA extraction has always been challenged through classification process. Therefore, efforts have been made to extract ISA from a variety of remote sensing data sources and through modeling. For example, sub-pixel methods have been developed for urban land classification (Ji and Jensen, 1999; Lu and Weng, 2004). A SPLIT model was developed (Wang and Zhang, 2004) to obtain ISA information through sub-pixel extraction by integration of Landsat TM and high spatial resolution digital multispectral videography data. Although this method is capable of extracting the percentage of ISA in mixed pixels, it is difficult to obtain a precise spatial distribution and coverage of ISA as

Department of Natural Resources Science, University of Rhode Island, 1 Greenhouse Road, Kingston, RI 02881 (ilikespoon@mail.uri.edu).

Photogrammetric Engineering & Remote Sensing
Vol. 74, No. 7, July 2008, pp. 857–868.

0099-1112/08/7407–0857/$3.00/0

needed. Estimations of ISA through the relationships between data from multiple sources have been used by the U.S. Environmental Protection Agency (EPA) and other researchers (Sleavin *et al.*, 2000; Yang *et al.*, 2003; Jennings *et al.*, 2004; Yang, 2006). The difficulty of using these methods is that the coefficient has to be established and validated for different study areas. Also the same challenge of precise coverage and accurate location of ISA remains. Therefore, extraction of ISA from high spatial resolution remote sensing data in meter or sub-meter level is in demand particularly by the planning agencies.

Although conventional pixel-based methods that have long been used for classification of moderate or low spatial resolution satellite remote sensing data can be used for classification of high spatial resolution data, the shortcomings are evident. The most noticeable is that the pixel-based classification will produce more dramatic salt-and-pepper effect due to the increased spatial resolution and noise level. Furthermore, the spatial information such as neighborhood, proximity and homogeneity can not be used sufficiently in these methods (Burnett and Blaschke, 2003). To conquer these problems and make sufficient use of spatial information from high spatial resolution data object-based classification has been developed (Baatz and Schäpe, 2000; Shackelford and Davis, 2003). Object-based methods simulate the process of human image understanding in feature extraction. It is especially suitable for processing high spatial resolution images. In addition, other spatial information can be integrated in modeling process. Object-based classification has been used in classification of high spatial resolution images and demonstrated the potentials (Blascheke and Strobl, 2001; Walter, 2004). The commercial software, such as eCoginition® (Definiens Imaging, Germany), is among the first object-based systems, and has been used for classification of high spatial resolution images (Wang *et al.*, 2004). Integration of high spatial resolution remote sensing and lidar data to extract impervious surface information has been studied (Hodgson *et al.*, 2003). Three image-object techniques, i.e., Fractal Net Evolution Approach, Linear Scale-Space, and Multiscale Object-Specific Analysis, were compared for analysis of landscape structure (Hay *et al.*, 2003).

An important step for object-based classification is to define regions in an image corresponding to objects in a ground scene. Successful image segmentation is the most important prerequisite (Baatz and Schäpe, 2000). The application of multi-scale segmentation in landscape analysis was discussed (Burnett and Blaschke, 2003). Segmentation algorithms, such as texture segmentation, watershed transformation and mean shift, have been developed in the past (Woodcock and Harward, 1992; Li *et al.*, 1999; Comanicu and Meer, 2002; Hu *et al.*, 2005), and a recent overview on image segmentation was summarized (Blaschke *et al.*, 2004). The segmentation results from high-resolution satellite imagery using several programs including eCognition® InfoPACK and CAESAR were compared and evaluated (Meinel and Neubert, 2004). As pointed by Baatz and Schäpe (2000), few of those methods lead to qualitatively convincing results that are robust and under operational setting applicable. Some of the methods are difficult for practical application because of the computing speed or the accuracy (Woodcock and Harward, 1992). In segmentation objects are grouped into larger homogeneous ones according to clustering cost functions adopted. In many segmentation algorithms using region growing, the entire process of image segmentation is completed in a single pass. These methods may produce large differences between pixels at opposite ends of a region. Woodcock and Harward (1992) developed a multiple-pass algorithm to extract forest information from Landsat TM data. This algorithm improved the segmentation of images from scenes better modeled as a nested hierarchy and achieved reasonable accuracies with the consideration of local best fitting and merging coefficient. The three advantages of this algorithm are as follows (Woodcock and Harward, 1992). First, it allows slow and careful growth of regions while inter-region distances are below a global threshold. Second, a minimum region size parameter can merge the regions with high variances. Third, maximum and variable region size parameters limit the merge of undesirable large regions. This approach can limit the rate of region growing in order to avoid the decision errors that arise as region centroids change due to premature segmentation merges (Woodcock and Harward, 1992). The mutual nearest neighbor principle used in the multiple-pass technique can produce more accurate region boundaries. However this algorithm was developed to process remote sensing data at 30 m spatial resolution. Further modification is necessary when dealing with high spatial resolution remote sensing imagery at meter or sub-meter levels. For example for high spatial resolution imagery, the shape information is an important measure in image segmentation and object-based classification, but it was not considered in the multiple-pass algorithm.

The classifiers used in the pixel-based classification can still be used in object-based methods. For example fuzzy logic is commonly used in object-based classification (Shackelford and Davis, 2003; Baatz *et al.*, 2004; Benz *et al.*, 2004). In order to use fuzzy logic, a rule-base must be established first. Subjective factors can be introduced in the process. Minimum distance and maximum likelihood are reliable classifiers and often used to make comparisons with other algorithms (El-Magd and Tanton, 2003; Reguzzoni *et al.*, 2003; Wang *et al.*, 2004). Minimum distance classifier can be used to build a rule base in fuzzy logic classification. Maximum likelihood classifier is a better one and more useful when prior knowledge is available and statistic criteria are taken into account. In some pixel-based classifiers, such as the maximum likelihood, the variability and relationship between spectral bands of the training pixels are considered. However, such information would not be available for a single pixel to be classified in these methods. In most of the existing object-based methods, such information was not considered. Therefore, it will be helpful for an object-based classification to include this type of information.

In this paper we developed a synthetic algorithm of multiple agent segmentation and classification (MASC) for extraction of ISA. The added shape information enhanced the multiple pass segmentation. The variability and relationship between spectral bands of the objects improved the classification accuracy. With GIS supported post-classification process, more precise ISA extraction was achieved from high spatial resolution remote sensing data. MASC allows us to modernize and enhance the existing GIS database and add new ISA data for the statewide GIS system, and to demonstrate a model that can be replicated for statistical and graphic comparison of ISA data from high spatial resolution remote sensing data.

Methods

Data Sources and Process

The State of Rhode Island is very much interested in searching for different methodologies and data sources to extract precise ISA information for the state, including using true-color digital orthophoto data and QuickBird-2 satellite imagery. The true color orthophoto dataset used in this study was acquired in 2003 by the Statewide Planning Program (SPP) through the National Agricultural Imagery Program (NAIP). This 1-meter ground sample distance

ortho-rectified imagery dataset has a horizontal accuracy of within ±3 meters of reference digital orthophoto quarter-quads (DOQQS) from the National Digital Ortho Program (NDOP). The orthophoto images are projected into Rhode Island State Plane Coordinate System with Zone 3800 in U.S. Survey feet. The resulting spatial resolution in this coordinate system is 1-meter (3.28 feet). The dataset has red, green and blue bands and distributed in GeoTIFF format (Plate 1a).

We also used the QuickBird-2 satellite data acquired on 29 April 2005 as the testing data. The QuickBird-2 image data were acquired for quantifying and identifying landscape characteristics related to impervious surface in a selected portion of the state. QuickBird-2 image data possess 0.6-meter spatial resolution on the panchromatic band and 2.5 m spatial resolution on the multispectral bands. The image data were projected to the same map coordinates as ortho-rectified, true-color aerial photos. Spatial resolution enhancement was performed through resolution merge of multispectral bands and sub-meter panchromatic band of QuickBird-2 imagery. After resolution merge the new dataset possesses 0.6-meter spatial resolution with four spectral bands covering the visible and near IR spectrum (Plate 1b).

Texture information is helpful for the definition of regions that have different levels of internal variance (Woodcock and Harward, 1992). We used a 3 × 3 window to extract the texture information of variance as one of the features in the segmentation process. We focused on two categories of ISA and none-ISA only for the classification process.

We selected a subset area of northern part of Narragansett in the east coast of Rhode Island (Plate 1c) as a primary testing area for algorithm development. This is a typical suburban community with intensive urban development. Residential and

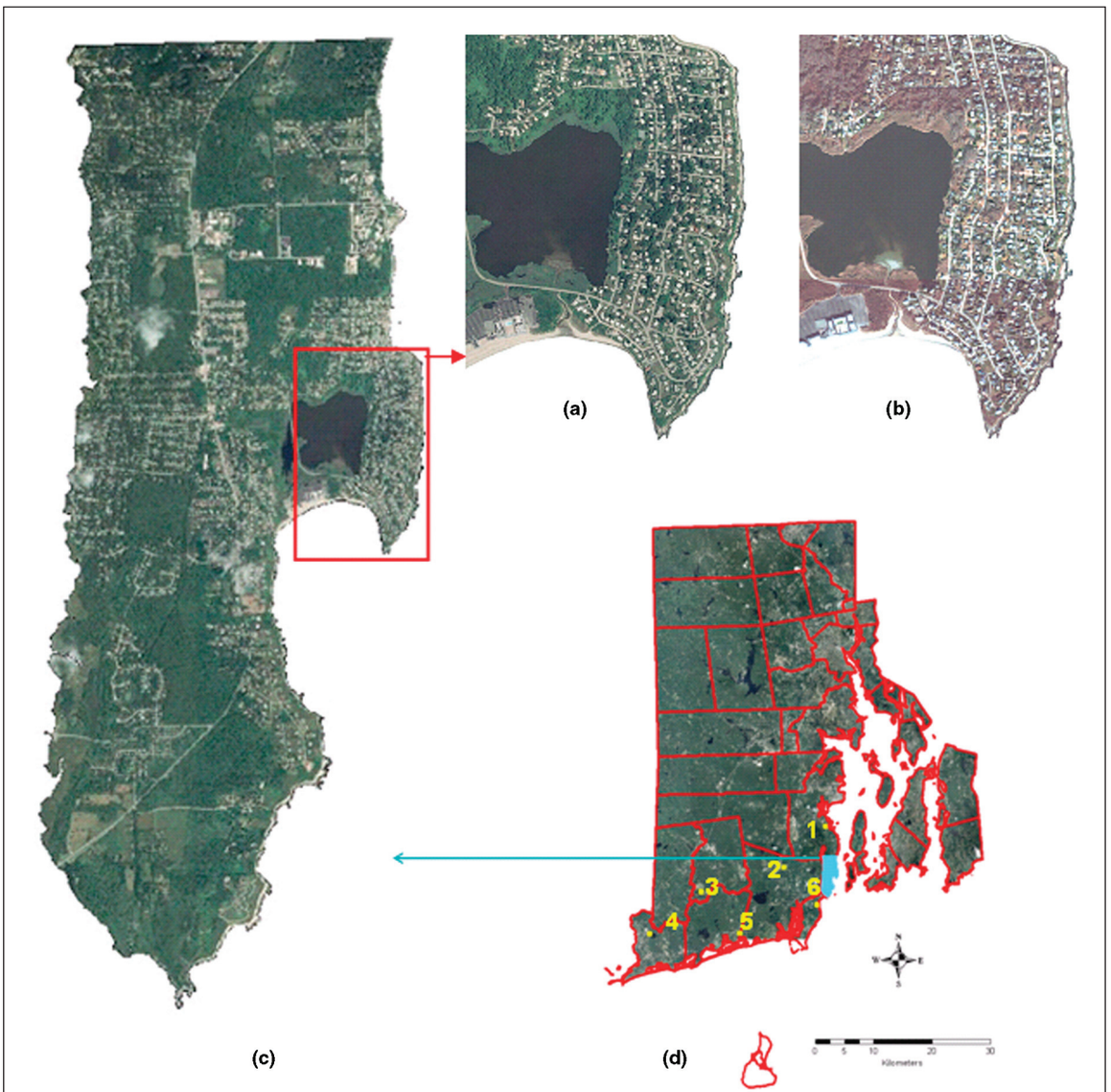

Plate 1. (a) An example of a true color digital orthophoto with 1-meter spatial resolution, (b) An example of resolution merged QuickBird-2 image with 0.6-meter spatial resolution and displayed as bands 3, 2, 1 in RGB, (c) The subset of the true color orthophoto for algorithm development, and (d) The locations of six selected testing sites for algorithm validation.

commercial areas are the representative landscapes. ISA are a major concern of this community in terms of watershed management and environmental monitoring. In addition, we selected six testing sites for MASC algorithm validation. Each site has different percentage of ISA cover in the southern coastal areas of the state. The locations of these testing sites are shown in Plate 1d. The orthophotos and QuickBird-2 images of these testing sites are shown in Plate 2.

Plate 2. Comparisons between true color orthophotos (upper image) and QuickBird-2 images (lower image) of the six selected testing sites for extraction of ISA in suburban environment: (a) Site 1, (b) Site 2, (c) Site 3, (d) Site 4, (e) Site 5, and (f) Site 6.

Multiple Agent Segmentation

The technical flow of the MASC algorithm is illustrated in Figure 1. We modified the multi-pass algorithm to accommodate the use of high spatial resolution digital imageries due to the finer pixel size and shadow effect. We developed a multiple agent segmentation sub-model (Figure 1a) that included spectral, texture and shape agents in this study and incorporated the shape information by heterogeneity change in place of spectral difference as the cost function for merging the regions. In the original multiple-pass algorithm, decision to merge two regions is based on the distance of channels in spectral space. In this study we used change of heterogeneity, i.e., combination of shape and spectral information to determine the merge of two regions. There are different possibilities to describe the change of heterogeneity before and after a merge. A common method for heterogeneity change is as follows.

The overall heterogeneity change h_{change} includes spectral, texture and shape agents:

$$h_{change} = \sum_{A=1}^{m+1+2} w_A \left(n_{obj1} \cdot (h_{A,m} - h_{A,obj1}) + n_{obj2} \cdot (h_{A,m} - h_{A,obj2})\right) \quad (1)$$

where h_{change} is the overall change of heterogeneity when two regions are merged, $h_{A,m}$ is a heterogeneity of the merged region for the agent A, $h_{A,obj1}$ and $h_{A,obj2}$ are the heterogeneities for two regions being merged for the agent A, n_{obj1} and n_{obj2} are the number of pixels in each of the two regions being merged, and w_A is the weight for each heterogeneity measure for the agent A (Shackelford and Davis, 2003; Baatz *et al.*, 2004). The agent can be spectral, texture, shape, color or other features.

In this study, we used three spectral channels from the true color orthophoto as $A = 1, 2, 3$ (i.e., $m = 3$, representing the number of spectral bands) for the heterogeneity measures described in Equation 1. We used the 4th channel ($A = 4$) for the texture component, and the 5th and 6th channels ($A = 5, 6$) for the shape components.

For dealing with the multispectral QuickBird-2 data, we used four spectral channels as $A = 1, 2, 3, 4$ (i.e., $m = 4$) for the heterogeneity measures described in Equation 1. We used the 5th channel ($A = 5$) for the texture component and the 6th and 7th channels ($A = 6, 7$) for the shape components.

The multiple pass algorithm can produce segmentations with minimal error by allowing merging to occur. In this merging process, at least spectral average heterogeneity of all image objects will increase. An image region is merged with the adjacent image region to produce minimum increase of heterogeneity. As for the adjacent regions, we adopted a four-way method (Woodcock and Harward, 1992).

In the segmentation sub-model, a merge process starts from single pixel objects and merges the small objects pairwise into larger ones. The ideal algorithm for a heterogeneity change metric Δh(obj1, obj2) for two regions was modified because only one merge per stage was allowed. The computing time is an important consideration for high spatial resolution remote sensing images. The multiple pass algorithm allows multiple merges per pass to minimize both the computing time per pass and the overall number of passes and keeps a minimum error of merging at the same time. In order to minimize the merging error and to improve the merging efficiency, two techniques were introduced, i.e., local mutual best fitting and merge coefficient (C_m) (Woodcock and Harward, 1992). The merge coefficient is used to calculate a histogram threshold for each pass. If n_{reg}

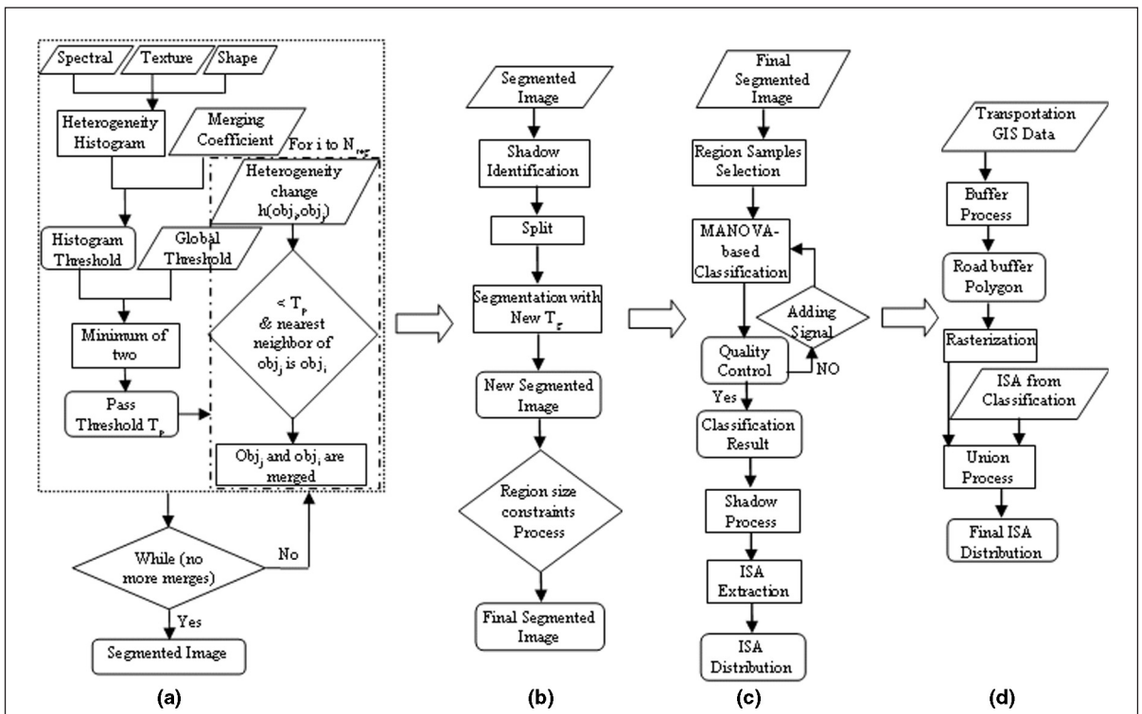

Figure 1. The flowchart of ISA extraction modeling: (a) segmentation sub-model, (b) shadow-effect sub-model, (c) classification sub-model, and (d) post-classification sub-model.

represents the current number of regions, the smallest heterogeneity changes for all n_{reg} regions are calculated and ordered. The new histogram threshold (T_h) is the heterogeneity change below which $C_m \times n_{reg}$ ordered heterogeneity changes lie. Therefore, there are two thresholds: global threshold (T_g) and T_h. The pass threshold (T_p) is defined as the minimum of T_g and T_h (Woodcock and Harward, 1992).

For orthophoto and QuickBird-2 imageries in this study, we used 2000 for the T_g; 0.95 for the C_m. We used 0.8 and 0.2 of w_A for spectral and shape components, respectively. We derived this set of parameters from the experiments on all of the testing images.

The shadows caused by tall vertical objects such as tree crowns are unavoidably associated with high spatial resolution imageries. The multiple pass algorithm had difficulty to differentiate shadowing areas. For example, tree crowns and shadows are always connected, overlapped, and hold insignificant spectral difference among them (Figure 2a). As the conventional multipass algorithm could not separate the tree crown and the ISA covered by the crown for the reason of spectral similarity (Figure 2b), we developed a split-and-merge method that is imbedded in the shadow effect sub-model for dealing with those types of mixed regions. The procedures of a shadow-effect sub-model are illustrated in Figure 1b. First, the mixed regions are identified based on the spectral feature of these regions. The mixed regions are separated into single pixels, and then the multiple pass algorithm is applied. A global threshold for this new segmentation was assigned a small value. The trees crowns and the shadows were segmented and the separated regions were identified (Figure 2c). Finally, the process of region constraint in the multiple pass algorithm was applied in the segmentation. In this study we used 80 for the T_g in shadow-effect sub-model based on the experiments in the testing images.

Classification and Post-classification

As a successfully segmented image was obtained after the initial and additional segmentation processes, the next step was to assign a class label to each of the regions on segmented image through a classification process. This process is shown in Figure 1c as the classification sub-model. We developed a new classifier on the segmented image in which the relationship between spectral bands and the variability in the training objects and those objects to be classified were taken into account.

This process allowed more information to be exploited in the single object. For example, in the maximum likelihood classification the variance and co-variance matrices of the training samples are used. In most of the existing object-based classification methods, the information of each spectral band is analyzed separately. If the observations were uncorrelated, these methods would be powerful. However, since spectral bands in remote sensing data are correlated, we developed a MANOVA-based algorithm that used the spectral distance to exploit such correlations. This would improve the result from univariate analysis which ignored the correlations among spectral bands and assumed independence of response variates. We used following distance equation (Equation 2) in the MANOVA-based classification algorithm:

$$\begin{cases} T^2 = \dfrac{n_1 n_2}{n_1 + n_2}(\bar{x}_1 - \bar{x}_2)^T S_p^{-1}(\bar{x}_1 - \bar{x}_2) \\ T^2_{adj} = \dfrac{n_1 + n_2 - p}{p(n_1 + n_2 - 2)} T^2 \end{cases} \tag{2}$$

where n_1 and n_2 are the numbers of the pixels in the object to be classified and training object, $\bar{x}_1$ and $\bar{x}_2$ are the mean spectral vectors of the object to be classified and training object, S_p is the pooled covariance based on two objects, p is the bands, T^2 is the distance between two objects, and T^2_{adj} is the distance with the consideration of the bands and pixels numbers.

Because of the special characteristics in the remote sensing data, hypothesis test based on F distribution in MANOVA is difficult to apply. We used Equation 3 to describe the quality of the classification result:

$$Q = \left(\sum_{i=1}^{n} \frac{D_{\min}}{D_i} - 1 \right) / n \tag{3}$$

where $D_{\min}$ is the minimum distance for all of the object classes, n is the number of the training samples, D_i is the distance for each of the object class, and Q is the quality index. The lower the index, the higher the classification quality.

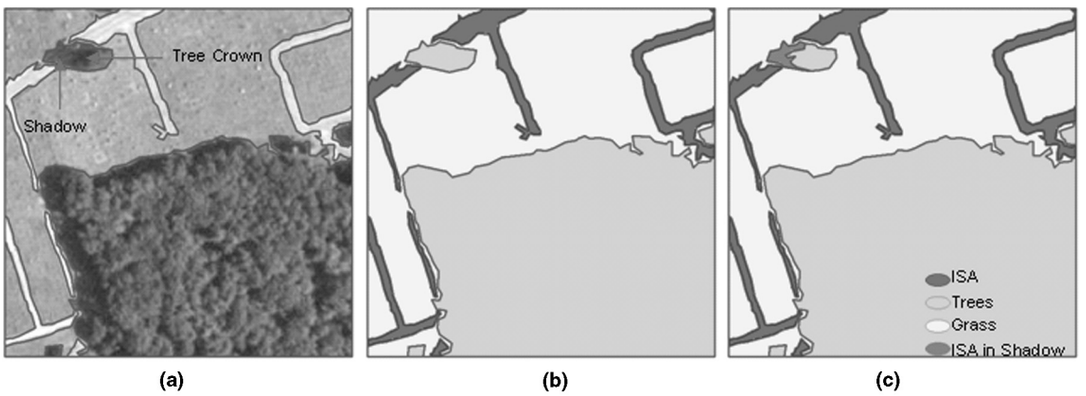

Figure 2. (a) An example of spectral similarity of tree crowns and the shadow in a true color orthophoto, (b) the result of image segmentation without considering the shadow effect, in which shadow covered ISA could not be separated from tree crowns that caused the shadows, and (c) the result of segmentation using the shadow-effect sub-model.

With added new training signals, the mean of quality index of the entire image scene decreased and reached a low level (Figure 3). We then applied a repeating algorithm based on the quality index. When the mean of quality index for the entire image is lower than the previous mean, a new object signal which has the largest quality index in the image was added into the training clusters. The classification stopped if the mean of quality index with the added signal was larger than the previous one.

The process was carried out as follows. First, the training samples for five main categories of ISA, forest, grass, soil, and water were established. Each category has several sub-categories. New sub-categories were added into the training samples based on the repeating algorithm, and these new samples were combined into the existing sub-categories or assigned new classes. After that the obtained classification result was recoded into ISA and none-ISA. We then used the ratio of the border length of the regions classified as shadow that are adjacent to impervious surface areas with all the border length to separate shadow-covered ISA and other land-cover types. This ratio varies with the sun azimuth and elevation angles. We derived the threshold for this ratio from a series of tests across the testing areas.

Upon finishing the classification we used the existing GIS data through a post-classification to extract ISA (Figure 1d) that were still not be identified through the process.

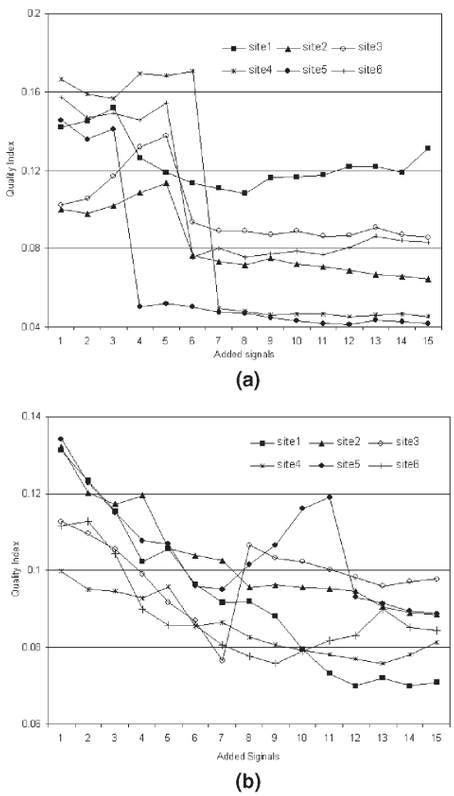

Figure 3. The quality indices from the six testing sites in (a) orthophoto, and (b) QuickBird-2 images responding to the added signals.

For example, some of the road segments are completely covered by tree crowns and are impossible to be separated on high spatial resolution imagery. We used a rasterized GIS transportation data as a reference to identify the road networks and integrated the road data with output from the classification sub-model to obtain the final ISA coverage. The post-classification warrants that the connected ISA is not interrupted and the final result represents the best information from both high spatial resolution remote sensing and GIS data.

Extending the Algorithm to the Entire State

The State of Rhode Island, except the Block Island, is covered by 113 scenes of digital orthophotos with 1-meter spatial resolution (Plate 1d). In order to extract the ISA for the entire state efficiently and quickly, we developed an automatic approach based on batch process and applied it on the segmentation and classification. First, the segmentation for this dataset was carried out using the same set of the parameters as the testing areas. With this process, 113 segmentation images were obtained. Second, the objects of training samples for certain land cover types were selected from this dataset. We compared and checked the data according to the covariance matrix of each object, and used the samples with smaller covariance. With this process we obtained the objects of training samples for each land cover type. Finally, an automatic approach was developed for the classification based on the batch process, and the results were recoded into ISA and none-ISA. The post-classification sub-model was then applied to obtain the high spatial resolution ISA covers for the entire state.

Results

The ISA extracted by different methodologies are illustrated in Figure 4. Visual comparison of the classification results reveals the differences between ISA from pixel-based algorithm and the MASC algorithm. Conventional pixel-based classification shows the salt-and-pepper effect in the testing area (Figure 4a) and an enlarged subset using the orthophoto (Figure 4b), as well as using QuickBird-2 image (Figure 4c). The MASC algorithm treated groups of pixels as the classification targets and achieved more accurate ISA coverage. Results in the testing area from the MASC algorithm is shown in Figure 4d, as well as the results derived from digital orthophoto (Figure 4e) and the QuickBird-2 image (Figure 4f) in the enlarged subset.

Because of the differences between object-based and pixel-based classifications, different accuracy assessments have been conducted (Herold *et al.*, 2002; Hay *et al.*, 2003; Shackelford and Davis, 2003). We used the random point sampling method to evaluate the classification accuracies in comparison between different classification methods on the orthophoto and QuickBird-2 data. We selected 200 samples and examined the classification accuracies for the ISA and none-ISA only. The confusion matrix indicates that the pixel-based classification achieved 86.5 percent overall accuracy using the orthophoto (Table 1). The producer's and user's accuracies are 82.1 percent and 78.6 percent for the ISA, and 88.7 percent and 90.8 percent for the none-ISA categories, respectively. The Kappa coefficient is 0.70. The MASC algorithm achieved a 92.5 percent overall accuracy using the orthophoto (Table 2). The producer accuracies are 82.1 percent and 97.7 percent for ISA and none-ISA categories. The user accuracies are 94.8 percent and 91.6 percent, respectively, with a 0.8259 Kappa coefficient.

The pixel-based classification achieved 87.5 percent overall accuracy using QuickBird-2 (Table 3). The producer accuracies are 70.6 percent and 93.3 percent for ISA and none-ISA categories. The user accuracies are 78.3 percent and 90.3 percent, respectively, with a 0.66 Kappa coefficient. The MASC algorithm achieved a 94 percent overall accuracy using QuickBird-2 (Table 4). The producer accuracies are 82.4 percent and 98 percent for ISA and none-ISA categories. The user accuracies are 93.3 percent and 94.2 percent, respectively, with a 0.8357 Kappa coefficient. The results indicate that the MASC algorithm performed better than pixel-based classification in ISA extraction from high spatial resolution data.

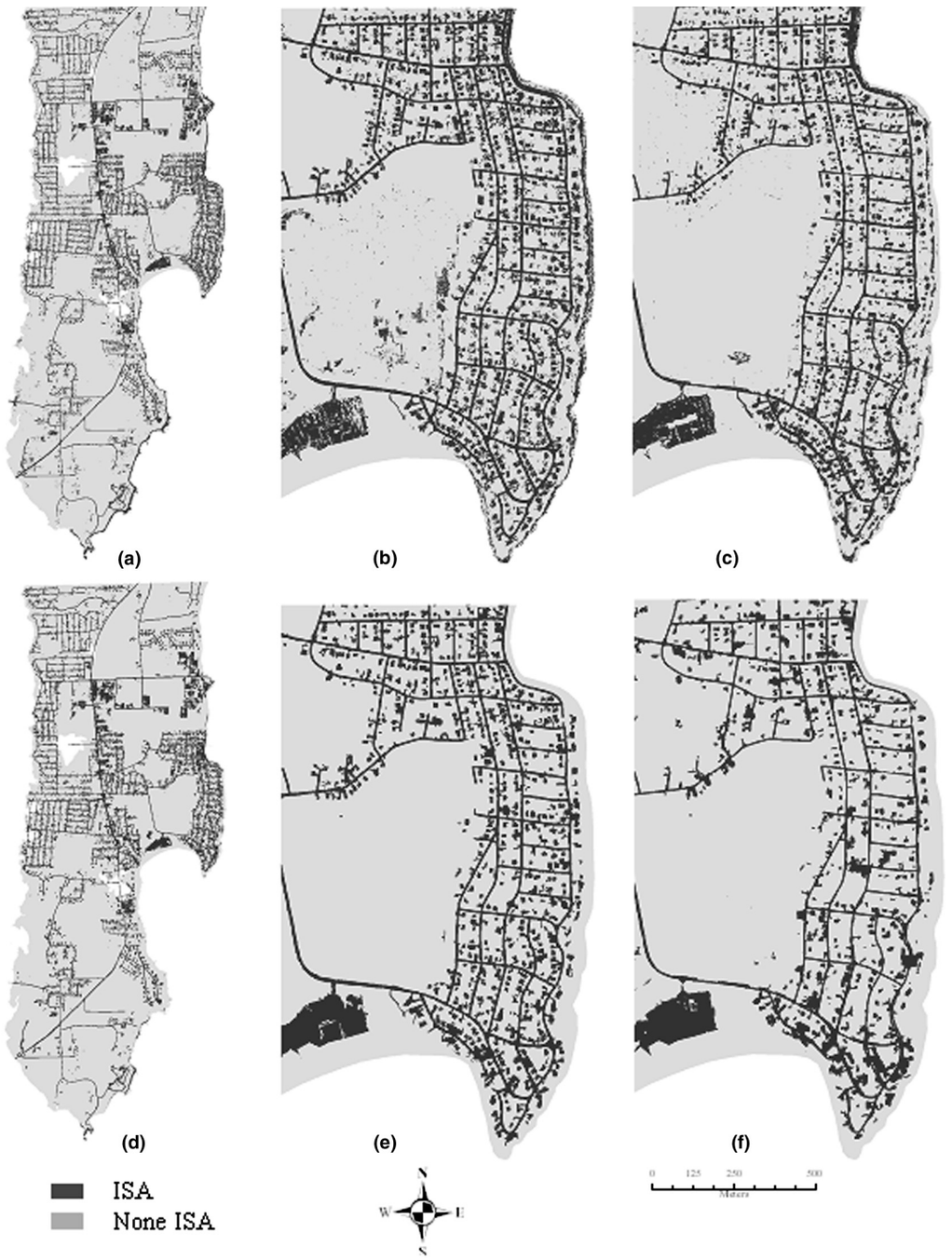

Figure 4. Extraction of ISA from the pixel-based method using (a) and (b) the true color orthophoto, (c) results from the pixel-based method using QuickBird-2 imagery, (d) and (e) results from MASC algorithm using true color Orthophoto and (f) results from the MASC algorithm using QuickBird-2 imagery.

TABLE 1. THE CONFUSION MATRIX BY PIXEL-BASED CLASSIFICATION USING ORTHOPHOTO

Algorithm Result \ Reference	ISA	none-ISA	Row Total	User's Accuracy %
ISA	55	15	70	78.6
none-ISA	12	118	130	90.8
Column Total	67	133	200	
Producer's Accuracy %	82.1	88.7		86.5

Kappa Value = 0.70
Overall Accuracy = 86.5%

TABLE 2. THE CONFUSION MATRIX BY MASC ALGORITHM USING ORTHOPHOTO

Algorithm Result \ Reference	ISA	none-ISA	Row Total	User's Accuracy %
ISA	55	3	58	94.8
none-ISA	12	130	142	91.6
Column Total	67	133	200	
Producer's Accuracy %	82.1	97.7		92.5

Kappa Value = 0.8259
Overall Accuracy = 92.5%

TABLE 3. THE CONFUSION MATRIX BY PIXEL-BASED CLASSIFICATION USING QUICKBIRD-2 IMAGERY

Algorithm Result \ Reference	ISA	none-ISA	Row Total	User's Accuracy %
ISA	36	10	46	78.3
none-ISA	15	139	154	90.3
Column Total	51	149	200	
Producer's Accuracy %	70.6	93.3		87.5

Kappa Value = 0.66
Overall Accuracy = 87.5%

TABLE 4. THE CONFUSION MATRIX BY MASC ALGORITHM USING QUICKBIRD-2 IMAGERY

Algorithm Result \ Reference	ISA	none-ISA	Row Total	User's Accuracy %
ISA	42	3	45	93.3
none-ISA	9	146	155	94.2
Column Total	51	149	100	
Producer's Accuracy %	82.4	98.0		94

Kappa Value = 0.8357
Overall Accuracy = 94%

We also evaluated the ISA extractions for the six selected validation areas for both the orthophoto and QuickBird-2 datasets using the MASC algorithm. The comparisons of the classification results are illustrated in Figure 5.

The result of extracted high spatial resolution ISA for the entire state is illustrated in Figure 6. As the first set of precise statewide ISA data, the map reveals the spatial distribution of ISA, in particular along the coastal line.

Conclusion and Discussion

This study developed a MASC algorithm that included sub-models of segmentation, shadow-effect, MANOVA-based classification, and post-classification. A nested-hierarchical model approach was used in the multiple pass algorithm. The segmentation sub-model replaced the spectral difference with parameters of heterogeneity change for merging regions. The shape information was introduced in the segmentation sub-model to enhance the performance of ISA extraction. In high spatial resolution images, particular in suburban settings, it is unavoidable that some of the ISA are covered by shadows of trees or buildings. The shadow-effect sub-model used a split-and-merge process to successfully separate shadows and the objects that cause the shadows. The classification sub-model used the MANOVA-based classifier so that the variability within the object and the relationship between the spectral bands were taken into account. For those areas that are completely covered by dense tree crowns GIS-based post-classification sub-model enabled the improvement of the ISA extraction.

Compared with the pixel-based method, the MASC algorithm achieved more precise and accurate information on ISA distribution. It eliminated the salt-and-pepper effect that is observable in the result from pixel-based method. In the MASC algorithm, spatial information such as neighborhood, proximity and homogeneity can be used effectively in the classification process. Fewer training samples are needed for this algorithm since each sample region contains multiple pixels and their spectral variations.

In pixel-based methods, the variability and relationship between spectral bands of the training samples are taken into account in some classifiers such as maximum likelihood. There was no such information for a single pixel in the pixels to be classified in those methods. In most of the existing object-based methods, the relationships between different spectral bands were not considered. Because of the correlations among different spectral bands in remote sensing data, it is helpful to exploit this relationship information in the data process. The MANOVA-based algorithm exploits the correlations of the spectral bands to explain the spectral distance between the training objects and those to be classified. In the MANOVA-based classification sub-model, a quality index was established to measure the classification quality. With this index and the repeating algorithm, the appropriate number of classes can be derived to get the best classification.

The MASC algorithm is successful in extraction of ISA from the high spatial resolution airborne true color digital orthophoto, as well as from space-borne multispectral image. True color orthophoto data are more common among state agencies and have been widely used by the general public. The QuickBird-2 data have advantages in multispectral coverage. The digital orthophoto data and spatially enhanced QuickBird-2 data possess comparable spatial resolution. The results from multiple testing areas, as well as from the entire state with different landscape and ISA characteristics, verified that this algorithm is applicable and robust. Therefore, the MASC algorithm can meet the requirements in high spatial resolution ISA extraction.

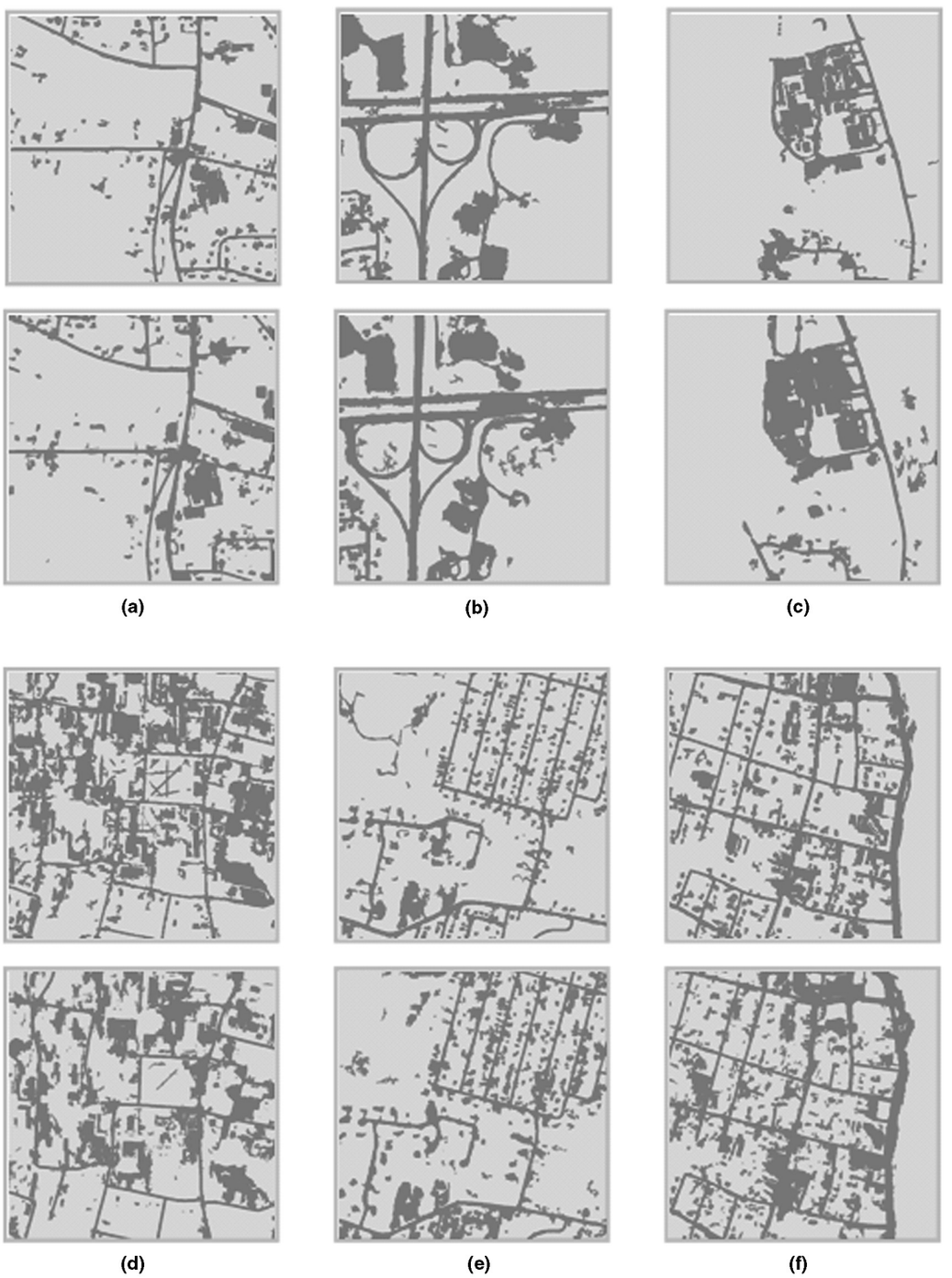

Figure 5. Comparison of ISA extraction for the six selected testing areas from (upper image) orthophotos and (lower image) QuickBird-2 images: (a) Site 1, (b) Site 2, (c) Site 3, (d) Site 4, (e) Site 5, and (f) Site 6.

The achieved ISA data should be the first state-wide high spatial resolution and precise ISA distribution that are available for the environmental impact studies. The data are also valuable in ecological and hydrological modeling to determine the impacting effects of land-use patterns on the coastal environment and watersheds.

Figure 6. Results of high spatial resolution ISA extraction for the State of Rhode Island.

Acknowledgments

This study was funded by the Rhode Island Agricultural Experimental Station (RI00H330). The QuickBird-2 data came from another project funded by the Institute for the Application of Geospatial Technology.

References

Arnold, C.A. Jr., and C.J. Gibbons, 1996. Impervious surface coverage: The emergence of a key urban environmental indicator, *Journal of the American Planning Association*, 62(2):243–258.

Baatz, M., and A. Schäpe, 2000. Multiresolution segmentation: An optimization approach for high quality multi-scale image segmentation, *Angewandte Geographische Informationsverarbeitung XII* (J. Strobl and T. Blaschke, editors), Wichmann-Verlag, Heidelberg, pp. 12–23.

Baatz, M., U. Benz, S. Dehghani, M. Heynen, A. Höltje, P. Hofmann, I. Lingenfelder, M. Mimler, M. Sohlbach, M. Weber, and G. Willhauck, 2004. *eCognition User Guide*, URL: *http://www.definiens-imaging.com*, Definiens Imaging, München, Germany (last date accessed: 26 February 2007).

Benz, U., P. Hofmann, G. Willhauck, I. Lingenfelder, and M. Heynen, 2004. Multi-resolution, object-oriented fuzzy analysis of remote sensing data for GIS-ready information, *ISPRS Journal of Photogrammetry and Remote Sensing*, 58 (3–4):239–258.

Blaschke, T., and J. Strobl, 2001. What's wrong with pixels?: Some recent developments interfacing remote sensing and GIS, *GeoBIT/GIS*, 6:12–17.

Blaschke, T., C. Burnett, and A. Pekkarinen, 2004. New contextual approaches using image segmentation for object-based classification, *Remote Sensing Image Analysis: Including the Spatial Domain* (S.M. de Jong and F.D. van der Meer, editors), Kluver Academic Publishers, Dordrecht, pp. 211–236.

Booth, D.B., and C.R. Jackson, 1997. Urbanization of aquatic systems: Degradation thresholds, stormwater detection, and the limits of mitigation, *Journal of American Water Resources Association*, 35(5):1077–1090.

Brabec, E., S. Schulte, and P.L. Richards, 2002. Impervious surfaces and water quality: A review of current literature and its implications for watershed planning, *Journal of Planning Literature*, 16(4):499–514.

Burnett, C., and T. Blaschke, 2003. A multi-scale segmentation/object relationship modelling methodology for landscape analysis, *Ecological Modelling*, 168(3):233–249.

Civco, D.L., J.D. Hurd, E.H. Wilson, C.L. Arnold, and S. Prisloe, 2002. Quantifying and describing urbanizing landscapes in the northeast United States, *Photogrammetric Engineering & Remote Sensing*, 68(10):1083–1090.

Comanicu, D., and P. Meer, 2002. Mean shift: A robust approach toward feature space analysis, *IEEE Transactions on Pattern Analysis and Machine Intelligence*, 24(5):603–619.

Dougherty, M., L.D. Randel, J.G. Scott, A.J. Claire, and G. Normand, 2004. Evaluation of impervious surface estimates in a rapidly urbanizing watershed, *Photogrammetric Engineering & Remote Sensing*, 70(11):1275–1284.

Draper, S.E., and S.G. Rao, 1986. Runoff prediction using remote sensing imagery, *Water Resources Bulletin*, 22(6):941–949.

El-Magd, I.A., and T.W. Tanton, 2003. Improvements in land use mapping for irrigated agriculture from satellite sensor data using a multi-stage maximum likelihood classification, *International Journal of Remote Sensing*, 24(21):4197–4206.

Hay, G., T. Blaschke, and D. Marceau, and A. Bouchard, 2003. A comparison of three image-object methods for the multiscale analysis of landscape structure, *ISPRS Journal of Photogrammetry and Remote Sensing*, 57(5–6):327–345.

Herold, M., A. Mueller, S. Guenter, and J. Scepan, 2002. Object-oriented mapping and analysis of urban land use/cover using IKONOS data, *Proceedings of the 22nd EARSEL Symposium*, 04–06 June, Prague, Czech Republic, The European Association of Remote Sensing Laboratories, pp. 531–538.

Hodgson, M.E., J.R. Jesen, J.A. Tullis, K.D. Riordan, and C.M. Archer, 2003. Synergistic use of lidar and color aerial photography for mapping urban parcel imperviousness, *Photogrammetric Engineering & Remote Sensing*, 69(9):973–980.

Hu, X.Y., C.V. Tao, and P. Björn, 2005. Automatic segmentation of high resolution satellite imagery by integrating texture, intensity and color features, *Photogrammetric Engineering & Remote Sensing*, 71(12):1399–1406.

Jennings, D., S.T. Jarnagin, and D. Ebert, 2004. A modeling approach for determining watershed impervious surface area from National Land Cover Data 92, *Photogrammetric Engineering & Remote Sensing*, 70(11):1295–1307.

Ji, M., and J.R. Jensen, 1999. Effectiveness of subpixel analysis in detecting and quantifying urban imperviousness from Landsat Thematic Mapper imagery, *Geocarto International*, 14(4):33–41.

Li, W., G.B. Benie, D.C. He, S.R. Wang, D. Ziou, Q. Gwyn, and J. Hugh, 1999. Watershed-based hierarchical SAR image segmentation, *International Journal of Remote Sensing*, 20(17):3378–3390.

Lu, D., and Q. Weng, 2004. Spectral mixture analysis of the urban landscape in Indianapolis with Landsat ETM+ imagery, *Photogrammetric Engineering & Remote Sensing*, 70(9):1053–1062.

Meinel, G., and M. Neubert, 2004. A comparison of segmentation programs for high resolution remote sensing data, *International Archives of Photogrammetry and Remote Sensing*, XXXV(Part B):1097–1105.

Novak, A., and Y. Wang, 2004. Effects of suburban sprawl on Rhode Island's forest: A Landsat view from 1972 to 1999, *Northeastern Naturalist*, 11(1):67–74.

Reguzzoni, M., F. Sanso, G. Venuti, and P.A. Brivio, 2003. Bayesian classification by data augmentation, *International Journal of Remote Sensing*, 24(20):3961–3981.

Schueler, T., 2003. *Impacts of Impervious Cover on Aquatic Systems*, Center for Watershed Protection (CWP), Ellicott City, Maryland, 142 p.

Shackelford, A.K, and C.H. Davis, 2003. A combined fuzzy pixel-based and object-based approach for classification of high-resolution multispectral data over urban areas, *IEEE Transactions on Geoscience and Remote Sensing*, 41(10):2354–2363.

Sleavin, W.J., D.L. Civco, S. Prisloe, and L. Giannotti, 2000. Measuring impervious surfaces for non-point source pollution modeling, *Proceedings of the ASPRS 2000 Annual Convention*, 22 – 26 May, Washington, D.C., American Society for Photogrammetry and Remote Sensing, Bethesda, Maryland, unpaginated CD-ROM.

Walter, V., 2004. Object-based classification of remote sensing data for change detection, *ISPRS Journal of Photogrammetry and Remote Sensing*, 58(3–4):225 – 238.

Wang, L., W.P. Sousa, and P. Gong, 2004. Integration of object-based and pixel-based classification for mapping mangroves with IKONOS imagery, *International Journal of Remote Sensing*, 25(1):1–14.

Wang, Y., and X. Zhang, 2004. A SPLIT model for extraction of subpixel impervious surface information, *Photogrammetric Engineering & Remote Sensing*, 70(7):821–828.

Weng, Q.H., 2001. Modeling urban growth effects on surface runoff with the integration of remote sensing and GIS, *Environmental Management*, 28(6):737–748.

Woodcock, C.E., and V.J. Harward, 1992. Nested-hierarchical scene models and image segmentation, *International Journal of Remote Sensing*, 13(16):3167–3187.

Yang, L., C. Huang, C.G Homer, B.K.Wylie, and M.J. Coan, 2003. An approach for mapping large-area impervious surfaces: Synergistic use of Landsat-7 ETM+ and high spatial resolution imagery, *Canadian Journal of Remote Sensing*, 29(2):230–240.

Yang, X., 2006. Estimating landscape imperviousness index from satellite imagery, *IEEE Geoscience and Remote Sensing Letters*, 3(1):6–9.

(Received 01 September 2006; accepted 09 November 2006; revised 06 December 2006)